A Method For Fabricating An Organic Photovoltaic Cell With Entirely 3D Printed Information Control

by

James Carter Minor

B.EngSci., University of Toronto (2015)

Submitted to the Department of Electrical Engineering and Computer Science
in partial fulfillment of the requirements for the degree of

Master of Science in Electrical Engineering

at the

MASSACHUSETTS INSTITUTE OF TECHNOLOGY

May 2020

Author . . . . . .
Department of Electrical Engineering and Computer Science
May 15, 2020

Certified by . . . . . .
Wojciech Matusik
Professor of Electrical Engineering and Computer Science
Thesis Supervisor

Certified by . . . . . .
Marc Baldo
Professor of Electrical Engineering and Computer Science
Thesis Supervisor

Accepted by . . . . . .
Leslie A. Kolodziejski
Professor of Electrical Engineering and Computer Science
Chair, Department Committee on Graduate Students

A Method For Fabricating An Organic Photovoltaic Cell With Entirely 3D Printed Information Control

by

James Carter Minor

Submitted to the Department of Electrical Engineering and Computer Science
on May 15, 2020, in partial fulfillment of the
requirements for the degree of
Master of Science in Electrical Engineering

Abstract

Advances in multi-material inkjet printing have enabled the creation of photovoltaic systems composed of entirely printed layers. These systems function by depositing all of the components of an organic (carbon-based) photovoltaic cell in liquid phase, and using heating to remove excess solvent between layer depositions. This thesis builds on those results, presenting a novel alternative to a traditional 3D printed silver top contact (which limits the performance of the photovoltaic cell with its high resistivity) in the form of an evaporated aluminum top contact whose geometry is determined by a 3D printed shadow mask layer. The shadow mask layer is composed of a 3D printed acrylate ink that is cross-linked under UV light, which can be removed after aluminum deposition to leave behind a tightly-controlled and well defined evaporated aluminum region. In this way, the author presents the first AM1.5 tested organic photovoltaic device with entirely 3D printed information control.

Thesis Supervisor: Wojciech Matusik
Title: Professor of Electrical Engineering and Computer Science

Thesis Supervisor: Marc Baldo
Title: Professor of Electrical Engineering and Computer Science

Acknowledgments

I would like to thank my advisors Wojciech Matusik and Marc Baldo for their invaluable technical guidance, support (both financial and emotional), and patience on this long project. I would also like to thank my labmates and MIT colleagues. In no particular order from that set, I am grateful to Mike Foshey, especially for printer construction and assistance in printer debugging, Wan Shou and Wenshou Wang, for chemistry advice, Tim Erps and Alexandre Kaspar for printer software design and selection, Anna Osherov for assistance in accessing CMSE facilities, Subramanian Sundaram for initial project design, and Ella Wassweiler for assistance in accessing ONE Lab facilities. Lastly, Cole Perkinson, Ting-An Lin, and Jan Tiepelt all helped me maintain the Angstrom aluminum evaporator. I'm also grateful for the use of ONE lab facilities, the CMSE shared testing facilities at MIT, and all my other colleagues in the CFG and Baldo group.

Additionally, I am deeply grateful to my undergraduate research advisor, Edward Sargent, for giving me my first chance to get involved in photovoltaics research, and my postdoctoral mentor and collaborator, Illan Kramer, for guiding me on my first major research project back at the University of Toronto.

Lastly, I couldn't have gotten this far without the guidance and love of my parents Joseph Minor and Christine Wilson, both of whom played a pivotal role in instilling in me a passion for learning that sustained me through the difficult times in my studies.

Contents

List of Figures

Chapter 1

Introduction and Related Work

The essence of this work is the attempt to combine two very distinct fields of engineering hardware development: 3D printing, and photovoltaics.

Additive manufacturing, also known as 3D printing, is a rapidly evolving field that is expanding from its origins in rapid prototyping to encompass bespoke product production [23], weight-minimizing part fabrication [15], and single-use item creation (such as models of organs of specific patients [18]). While the earliest kinds of 3D printing (stereolithography and fused deposition modeling) were limited to printing certain kinds of plastics, more recent technologies have dramatically expanded the range of printable materials, encompassing metals (often through selective laser sintering), composites (often through laminated object manufacturing), and many others. For a complete break-down of the major types of 3D printing, see Fig. 3 of [25].

This thesis will focus on building devices using a custom Polyjet system called MultiFab [21] created by the Computational Fabrication Group (CFG) in the Computer Science and Artificial Intelligence Laboratory (CSAIL) at the Massachusetts Institute of Technology (MIT). Like all Polyjet systems, MultiFab uses inkjet printheads to deposit droplets layer by layer. However, while our most commonly used materials are rigid and elastic photopolymers cured under UV light (called RIG and ELA, respectively), we have managed to produce a wide range of materials that can be printed on our system, from layers of silver to hydrogels to transparent conducting layers based made of poly(3,4-

ethylenedioxythiophene)-poly(styrenesulfonate) (commonly known as PEDOT:PSS), many of which rely on air or heat curing rather than UV light. MultiFab is therefore a flexible multi-material 3D printing platform, capable of printing liquids with viscosities in the 2-15 cps range and surface tensions in the 30-40 nM/m range. This system's standard minimum-resolution voxel size is 40 μm by 40 μm by 20 μm, but in practice its z-dimension can be reduced significantly for any printed solution whose solvent can be induced to evaporate after printing (either through inherent volatility or with use of a heating element) [21].

Using this system, the original goal of this thesis was be to create a full 3D printed organic photovoltaic device (solar cell), which will initially be used as the basic building block in constructing arrays of light sensors that can be arranged in novel architectures [11] [14]. The longer-term goal of the work is to add a stable, consistent light sensor to the group's library of printable devices, complementing work done on strain sensors [22], printed transistors [22], printed actuators, and magnetic panels, as well as to potentially enable the creation of large photovoltaic devices on surfaces with multiple axes of curvature (existing photovoltaic manufacturing techniques tend to be limited to planar surfaces or a single axis of curvature due to their lack of surface independent conformal coating capabilities [13], thus precluding their deployment on car roofs or any other aerodynamically constrained application).

All solar cells that are currently commercially available are crystalline, and thus unprintable in our system. However, so-called third generation solar cells (first generation being crystalline silicon, second generation being thin-film crystals such as CdTe or CIGS [24]) have mostly or entirely solution-processed fabrication methods, which means they are likely printable on the MultiFab system (if their components can be modified to fall within the necessary surface tension and viscosity ranges). The three types of third-generation solar cells are quantum dots [17], organic solar cells [5]] and perovskites [16]. Although perovskites are the most novel (and the most active area of research at the moment), their extreme sensitivity to slight changes in the manufacturing process would make them extremely challenging to print. Similarly, quantum dots tend to require ligand exchange to occur after deposition [12], making their fabrication process chemically messy and logistically difficult, as it would require using multiple inks and potentially flooding the print

surface to remove excess ligands. Therefore, this thesis will focus on fabricating entirely inkjet-printed organic solar cells.

There have been a few recent efforts to fully or nearly fully print an organic based photodetector or solar cell [2] [3] [9] . Of these, [9] was selected for imitation due to its fully-air stable process, as well as its similarity to my existing control devices, which are standard spin-coated P3HT:PCBM based devices similar to the ones outlined in [20]. These control devices were selected due to their incorporation of PEDOT:PSS (a material whose printing parameters were already known to the group [22]), as well as P3HT's stability, reliability, and well-known properties within the organic solar community. It should be noted that an initial attempt to print P3HT:ICBA devices (based on [8]) failed due to the mixture of the P3HT and ICBA with ethanol being an unstable suspension rather than a true solution.

Thus, the original focus of this thesis was to create a fully printed stack consisting of:

a) a translucent substrate of RIG

b) a bottom contact / cathode of PEDOT:PSS (where the holes will exit the device)

c) an active / absorber layer of poly[N-9‘- heptadecanyl-2,7-carbazole-alt-5,5-(4‘,7‘-di-2-thienyl-2‘,1‘,3‘- benzothiadiazole)] (PCDTBT) and [6,6]-phenyl-C71-butyric acid methyl ester (PCBM) mixed together in a bulk heterojunction

d) an electron transport layer of zinc oxide (ZnO)

e) a top contact / anode of commercial inkjet-compatible silver ink

In the above architecture, the ZnO layer both acts as an electron transport layer (increasing device efficiency by aiding the extraction of electrons) and acts as an interface between the active layer and the top contact, making printing a relatively hydrophilic compound (the silver ink) on top of a hydrophobic surface (the active layer) easier.

However, difficulties (that will be discussed in the Analysis section) prevented the realization of this original course of action. Fortunately, exploring them opened up a new, more technically promising pathway. The ZnO layer was replaced with a 3D printed removable shadowmask layer, and the silver ink was replaced with an evaporated aluminum layer. So the revised device structure was:

a) a translucent substrate of ITO coated glass

b) a bottom contact / cathode of PEDOT:PSS (where the holes will exit the device)

c) an active / absorber layer of poly[N-9‘- heptadecanyl-2,7-carbazole-alt-5,5-(4‘,7‘-di-2-thienyl-2‘,1‘,3‘- benzothiadiazole)] (PCDTBT) and [6,6]-phenyl-C71-butyric acid methyl ester (PCBM) mixed together in a bulk heterojunction

d) a removable acrylic 3D printed shadow mask

e) a top contact / anode of evaporated aluminum

This is an interesting pathway for exploration, because, while there have been recent efforts to fully print photodiode arrays with silver nanoparticles and a zinc oxide blocking layer [6], deposit a carbon nanotube film by spraying through a shadow mask [7], and use a shadow mask to pattern spray-coated PEDOT:PSS contacts [19], the only work that was analogous to our efforts was [10]. In [10], the authors used a similar shadow mask method to produce light sensors. As we will see in the Results and Discussion section, my approach differs in its efficiency, as well as the fact that all the layers of my device below the shadow mask are printed, whereas the layers below the shadow mask in [10] are stamped.

1.1 Overview

In this chapter, I have gone over the background of this project, as well as some related work. In chapter 2, I detail the hardware platforms used to create the devices made in the course of this project. In chapter 3 I detail the procedures for creating said devices. In chapter 4, I describe how the performance of the devices was evaluated. In chapter 5, I describe the challenges faced in the course of this project. In chapter 6, I detail the results of characterization of the final, working device and discuss the outcome of this project. Finally in chapter 7 I discuss possible avenues for future exploration.

Chapter 2

Fabrication Platforms

The devices created in this project were fabricated using a combination of two print platforms and one metal evaporator.

The first print platform was the Multifab print system developed by the Computational Fabrication Group here at MIT [21]. This print system uses inexpensive, easily replaceable Epson Workforce 30 printheads (approximate unit cost $40 / printhead) to allow for a range of experimental fluids to be printed. As the analysis section will discuss, this print system was incompatible with the chlorinated solvents required to print certain layers of the device, and so for the final output it was only used to print the acrylate based peel-off shadow mask.

The system has 5 channels, 2 containing 180 nozzles and 3 containing 60 nozzles. It maintains negative pressure during printing to prevent the ink from dripping out of the (always open) print nozzles. Terminology note: "purging" refers to the process of applying a strong forward pressure to force ink from the reservoir down through the tubing out the front of the printhead. Once the ink has reached the front of the printhead and is dripping out, negative pressure is restored and the excess ink is wiped off the front face. On the Multifab, this wiping process is done by mechanically moving the printhead over flexible rubber ridges that physically remove the excess ink, which then runs down the sides of the ridges into a waste reservoir. When a printhead started to clog (had some of its 540 nozzles cease to function), it would be removed, thrown out, and replaced with another printhead (which cost approximately $40). This printer has a resolution of approximately 40 μm in

x by 40 μm in y by 20 μm in z, where z is the vertical axis. These dimensions are for the deposition of acrylate based fluids that are well characterized for this printer. This printer can be used to successfully deposit PEDOT:PSS as well, but its dimensions for this task are different, especially in z, since the PEDOT:PSS fluid is a water-based solvent where 99% of the mass of the deposited fluid evaporates after deposition, whereas the acrylate based fluids are UV-cross-linked, meaning that after deposition a UV light is shone on them and they transition from a liquid phase to a solid phase because the UV light stimulates fiber cross-linking, a process which is discussed more in depth in [21].

The second print platform is a printer also developed by the Computational Fabrication Group here at MIT, based on the Nordson PicoPulse printhead. The key advantage of this print system is its entirely stainless steel and ceramic print pathway, which allows it to survive prolonged operation with aggressive solvents. This printer was used to print the transparent hole conducting layer (PEDOT:PSS, water based solvent) and the light-absorbing bulk heterojunction layer (PCDTBT + PCBM, chlorinated solvents).

This printhead would be cleaned through immersion in a solvent, plus sonication in an ultra-sonicator. For PEDOT:PSS printing, it was subsequently cleaned through immersion in ethanol + sonication of the container containing the printhead and the ethanol, usually for about 5 minutes. For active layer printing, it was first cleaned through immersion + sonication in chlorobenzene for 5 minutes, then through immersion + sonication in ethanol for 5 minutes. If chlorobenzene + ethanol proved insufficient, it was also immersed + sonicated in acetone for 20 minutes. Note that the O-ring that is used in this printhead is sensitive to acetone and so the part containing the O-ring should not be immersed in acetone, since it will cause the O-ring to swell and over repeated cycles will damage it. This is not a problem for the cleaning process since the large stainless steel and ceramic portion of the printhead is the part that is most difficult and important to clean.

Additional cleaning notes: after immersing the printhead in a fluid, you should use compressed air (we used standard compressed air bottles with small plastic nozzles for reaching into the parts) to dry the parts, since that will help remove any fluid still containing contaminants. If after compressed air purging the printhead appears to still have staining on it, it is recommended that you repeat the last fluid step, after wiping the affected sections

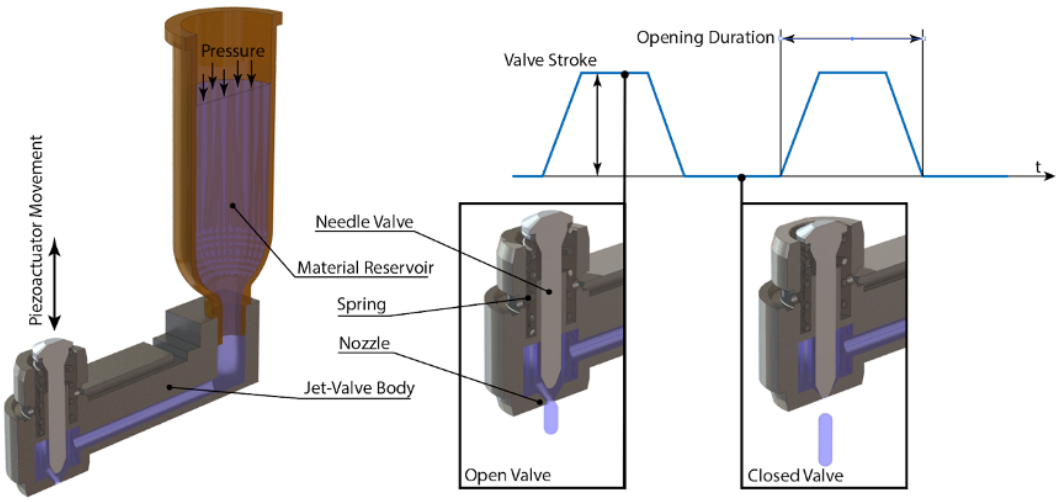

Figure 2-1: Left: a layout of the PicoPulse printhead, with the fluid/varnish reservoir and print pathway clearly labelled. Bottom right: details of the droplet extrusion process. Top right: depiction of the applied voltage to open the printhead to extrude a droplet.

with a kimwipe soaked in that same fluid to see if physical abrasion can remove them. On rare occasions, the internal pathway in the large printhead part will develop a blockage that needs to be physically pushed through using a metal wire. You can determine that this is the case by using a squeeze bottle nozzle to push fluid from one side of the printhead through to the other. If it doesn't go through, there is an internal blockage that requires physical force to remove.

After cleaning, the printhead should be confirmed to be ready for printing by examining its print nozzle in an optical microscope. Its print nozzle is a 50 μm circle, which should be entirely free of blockages when you illuminate it from the bottom. Notes on this process: To stabilize the printhead to allow for easy viewing, you can use the fact that its print surface is parallel to the top of screw nozzle connection. By flipping the printhead upside down, you can press the top of the screw nozzle to the surface of the microscope platform with one hand, which stabilizes the printhead in place (maintain pressure while viewing to prevent motion). Then, use top illumination to identify the location of the nozzle, zoom to maximum magnification, then turn off top illumination and turn on bottom illumination. You should see a fully lit circle that goes dark when you pass a piece of paper between the printhead and the viewing lens.

The metal evaporator used was an Angstrom metal evaporator system. This system was

Figure 2-2: Diagram of the PicoPulse controller (left), PicoPulse printhead mounted in place (bottom) and fluid reservoir (right, clear tube).

used to deposit the aluminum top contact as a uniform coating, resulting in a patterned aluminum deposition on the actual device once the acrylate mask was removed. The deposition rate of the aluminum was 2 Å/s, resulting in a deposition time of 500s for the 100nm (1000 Å) layer. Other fabrication parameters: the aluminum layer was preheated before deposition to ensure a steady rate of deposition when the substrate shutter was open. The power setting necessary to achieve this will vary system to system, but for the Angstrom evaporator used in this project, the pre-heating protocol was to heat at 55% power for 5 minutes, then to do an autotuning protocol for approximately 2 minutes, followed by a stabilization protocol for 2 minutes to establish what power setting at steady state was sufficient to produce a 2 Å/s deposition rate (usually 68% power). The control samples were taped to a machined metal mask, which was placed in the chamber facing downwards above the aluminum source.

Chapter 3

Device Fabrication

The devices developed in this process follow a standard (non-inverted) bulk heterojunction organic photovoltaic (OPV) model, as seen in [9]. This stack uses 12.7mm x 12.7mm glass wafers with 0.7mm thickness with an Indium-Tin-Oxide (ITO) pattern deposited on the top. The ITO layer is used to boost efficiency to increase the ease of identifying working devices at early stages of the project but is not necessary for device functionality. The ITO slides were purchased from Thin Film Devices of Anaheim, California. Their complete specifications, along with an example order form, are given in Appendix A. The layout of the patterned ITO on the glass is a pattern called # MIT 554, and its layout is shown in Figure 3-1.

On top of this patterned ITO is deposited the poly(3,4-ethylenedioxythiophene) polystyrene sulfonate (more commonly referred to as PEDOT:PSS) layer using the PicoPulse printhead printer, whose print conditions are given in below. After deposition, this layer is dried for 15 minutes at 120 degrees Celsius on an IKA RCT Basic hotplate. The PEDOT:PSS is Heraeus Clevios PH-1000.

On top of this PEDOT:PSS layer is deposited the light-absorbing bulk heterojunction layer (PCDTBT + PCBM, chlorinated solvents), generally referred to hereafter as the active layer. This deposition also occurs on the PicoPulse printhead printer. Its print conditions are given below. After deposition, this layer is dried for 10 minutes at 70 degrees Celsius on an IKA RCT Basic hotplate.

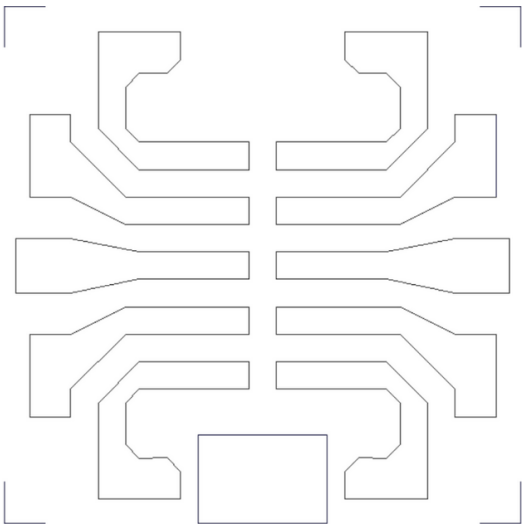

Figure 3-1: Layout of the patterned ITO on the glass slides used to fabricate my devices The enclosed regions denote areas of ITO deposition. The corners indicate where the corners of the glass slide would be. For complete specifications of electrical properties, see Appendix A.

Then the shadow mask blocking layer is deposited according to the pattern shown in Figure 3-4 using the multifab printer. The shadow mask layer consists of an acrylate mixture made in our lab called RIG7.9.

Lastly, aluminum was deposited using the Angstrom evaporator. The aluminum layer was 100nm of aluminum, deposited uniformly at a rate of 0.2 nm / s.

3.1 Print Conditions for PEDOT:PSS and Active Layer

70 psi, 100V, 55% on glass [+7% for printing on active layer] stroke, 0.25ms Open, 0.5ms Close, 0.27ms pulse, 5ms Cycle, Count 1, print file saved to my directory in the GitHub as "20200110-Print1.txt", Ink reservoir somewhere between 5 degrees C (refrigerator temp) and room temp, print surface at room temperature, printhead at . room temperature. PEDOT filtered through 1um glass filter. 4mL in ink reservoir. Ink C11 PEDOT. Sash position 1. Move directly onto 120 degree heat once done printing. 15 minutes heating.

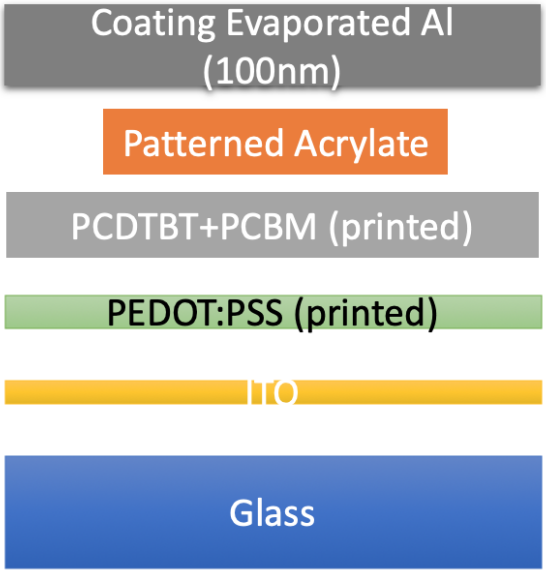

Figure 3-2: Diagram detailed the layers of the fabrication process. The ITO-patterned glass (bottom) is first deposited with PEDOT:PSS (green), then with PCDTBT+PCBM (light gray), then the shadow mask (pattern acrylate, orange) is put into place. Then the top layer of evaporated aluminum (dark grey) is deposited. Then the shadow mask is removed, the process of which is detailed in 3-3

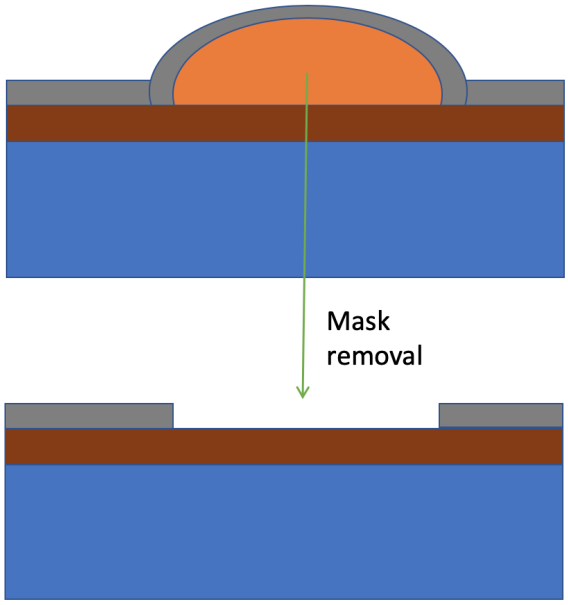

Figure 3-3: The shadow mask (orange) is put into place on top of the PCDTBT:PCBM (brown) active layer before deposition of the aluminum layer (gray) by evaporation. Afterwards, it is removed, along with the aluminum that was deposited on top of it, leaving aluminum only in the regions where it was not present.

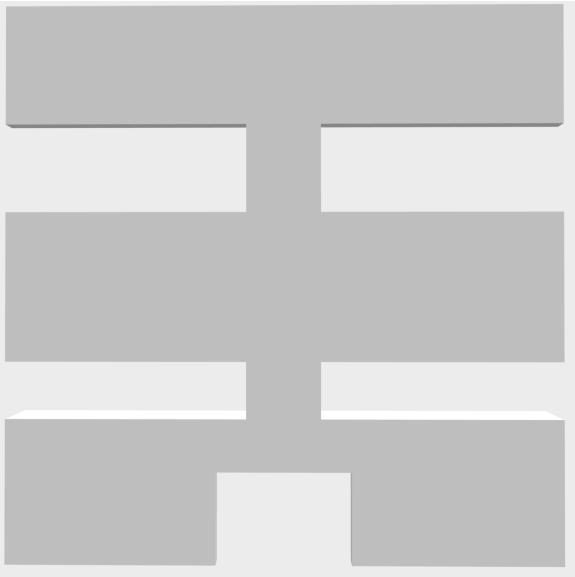

Figure 3-4: The deposition pattern of the shadow mask. Scaled to the same 12.7 mm x 12.7mm template as my ITO pattern. The darker gray area indicates the area covered by the shadow mask. The basic operation of the shadow mask is shown in Figure 3-3

3.2 Print Conditions for Active Layer

0.40ms pulse, printhead, ink reservoir all at room temperature, 0.25ms open, 0.24ms close, 60 psi, 55% stroke, FILTERED 1um glass filter.Count = 1. Cycle = 5ms, Frequency = 200 Hz. Acetone wipe beforehand. Sash at max openness (formerly position 1). REMINDER: SPREADING DIFFERENT ON PEDOT vs Bare Glass. Printed on a heated surface at 70 degrees. Moved onto 70 degree hotplate for 10 minutes immediately afterwards. NOTE: SENSITIVE TO Z-SPACING, TURNED THE PRESSURE TO ZERO AFTER PURGING

Chapter 4

Device Characterization

Device characterization was done using an iPhone 8 camera, an optical microsope, an SEM system, and a custom solar simulator constructed by the ONE lab at MIT, which conforms to the standard AM1.5 testing standard. The crucial IV curve data was collected on this solar simulator.

This droplet spacing study is included here to demonstrate the visual signatures of droplet spacing in a print. On the right, we have a droplet spacing that is too high, resulting separation between droplets. This separation also causes excess fluid to build up in irregular unpredictable patterns. By contrast, the center print is right at the critical threshold where droplets merge but don't overlap on impact. The left print has droplets even closer together, resulting in liquid droplets colliding chaotically on impact and spraying small satellite droplets into the surrounding area (clearly visible as the small dots present

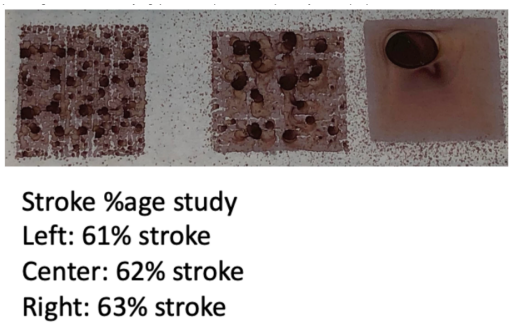

Figure 4-1: A study showing the impact of stroke % changing on film quality.

Droplet spacing study.
Left: 0.25mm x 0.25mm droplet spacing
Center: 0.35mm x 0.35mm
Right: 0.45 x 0.45mm (note droplet separation)

Figure 4-2: A study showing the impact of droplet spacing on film quality.

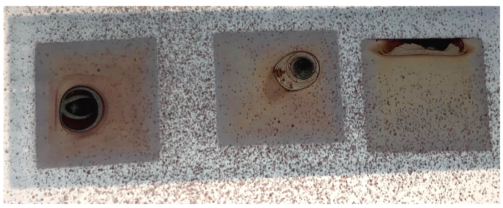

Temperature printing study.
Left: Room temperature print + dry
Center: Room temperature print, dry at 70 degrees
Right: Print + dry at 70 degrees

Figure 4-3: A study showing the impact of heating conditions on film quality.

surrounding the square print area.

Printing onto a 70 degree print surface produces the best film quality because it evaporates much of the solvent during the printing process, preventing a large pool from building up in the center of the print (the circular patches in the left and middle). Instead, with careful printing control, excess fluid ends up on the edge of the print (the line on the top of the right square), outside the region used to produce devices. Note that the active layer is highly sensitive to temperature – it can survive being heated to 80 degrees for 24 hours, but will be destroyed (produce shorted devices) if heated to 100 degrees for 5 minutes. Note that satellite droplets are present for all three prints.

Chapter 5

Analysis

5.1 Silver Ink Shorting Behavior

On the way to developing the final approach outlined in this thesis, many attempts were made to produce an entirely printed solar cell using silver nanoparticle inks. There have been prior reported successes at this approach, most notably [9]. However, my attempts to replicate them ran into persistent difficulty in producing non-shorted devices. Although the silver inks in question could be printed on both the multifab and PicoPulse print platforms, any time silver ink was used it would produce a shorted device.

Curiously, these shorted devices did not visually appear to have eaten through the (very thin) active layer (optical microscopy didn't reveal any macroscale defects), which suggests that the shorting was due to a chemical infiltration. This was surprising, because the same shorting behavior occurred across several different solvent types. Over the course of the project I attempted printing using the silver ink formulation from [21], the silver ink from [9], a xylene based silver ink from UT-Dots called AgX, and a trio of silver inks printed by the aerosol jet company Optomec (silver inks "Nagase", "ANP", and "EI"). The continued shorting behavior of the last 3 was especially surprising, because optical microscopy supported the fact that the silver droplets of the Optomec print system (located in Minneapolis) mostly dried in flight on the way to the device surface, producing a silver film that was conductive edge to edge but had many micro-holes where droplets had not landed (there was

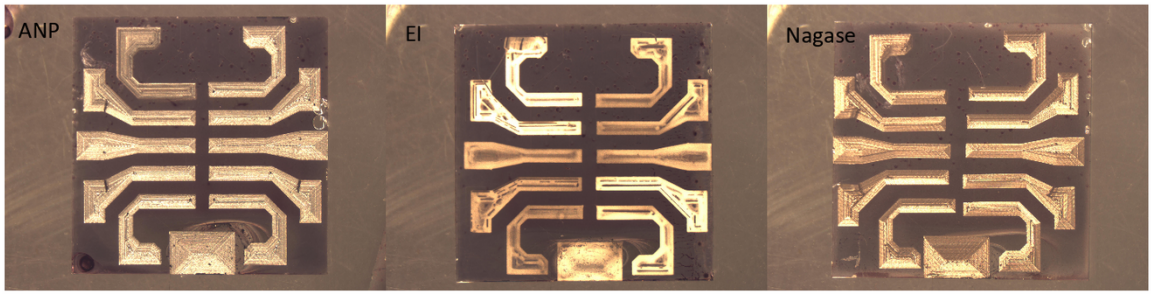

Figure 5-1: Three devices produced with silver ink deposited from the Optomec Aerosol Jet Print system. Left "ANP", center "EI", right "Nagase".

no post-impact liquid spreading phase).

The key difference between my attempts and the Sirringhaus paper is that the Sirringhaus paper had a custom zinc oxide blocking layer protecting its active layer from the silver ink that it used. Because this was a custom zinc oxide layer that was not fully specified in the source papers (partially specified in [4] and [9], with several key details missing), I was unable to replicate it perfectly despite a variety of attempts to do so. This drove me to experiment with the acrylate shadow mask technique which ended up being my crucial contribution. Of note, my experimentation couldn't rule out the possibility that the actual silver nanoparticles themselves were the root cause of the shorting behavior, and it should be noted that organic photovoltaics and LEDs are well documented to fail when silver is attempted to be evaporated onto them.

5.2 Multifab Printing Difficulties

Another stumbling block to be noted for future students of similar projects is that there was an extended period of difficulty in printing the active layer on the multifab printer. This was because, which the ink could be loaded and would print, the printing behavior was incredibly unstable, only printing even somewhat for 5-10 minutes after loading (and then not perfectly stably) before clogging and requiring a replacement printhead to be installed. It took quite a while to determine that the root problem of this wasn't printing parameters (as the Epsom ink printhead often required extensive fine-tuning to produce good printing parameters, and the experimentation on this was hampered by the expense and limited

quantity of the active layer reagents), but was in fact a chemical reaction between the reactive chlorinated solvents of the active layer inks and some of the internal plastic components of the Epsom printheads, which contained small filters and other delicate components that could be easily degraded by chlorinated solvents. In contrast, once the transition was made to the newer PicoPulse printhead printer system, successful prints with the active layer were produced in relatively short order. The key difference was that the PicoPulse printhead's print pathway was entirely stainless steel and ceramic, both sturdy, chemically non-reactive components. The only plastic-solvent interface for printing the active layer was in the syringe containing the fluid (see Figure 2-1) and the combination of durable plastic, limited surface area, and not being on the critical print pathway prevented it from hampering the printing process. The downside of migrating to the PicoPulse printhead system is that it has a much larger minimum droplet size than the MultiFab print system.

5.3 PicoPulse Printing Limitations

While the MultiFab print system can consistently perform prints with droplets measuring only 40 μm by 40 μm, the minimum droplet size of the PicoPulse is more like 250 μm by 250 μm and in practice often closer to 500 μm by 500 μm. This resolution limitation is the cause of some of the odd printing parameters of the active layer on the PicoPulse, such as switching off the pressure to the printhead after purging. Not having back pressure significantly reduces the minimum stable droplet size, but it means that when you print you aren't fully "replacing" the fluid at or close to the printer nozzle. After you purge with the pressure on to force a lot of fluid through and then turn the pressure off, the first one or two prints will be extremely messy (because there is too much fluid near the print nozzle.

Chapter 6

Results and Discussion

Note: characterization of the final result devices is somewhat limited, because the lab had to shut down due to COVID-19. The first working devices with the shadowmask technique were tested on March 17th, the last day that the Organic and Nanostructured Electronics lab was open.

Two working devices were produced using the shadow mask deposition method. Their electrical results are given in Figures 6-2 and 6-3. The device has a power conversion efficiency (ratio of power collected divided by power delivered) of 0.08%.

Having obtained the power conversion efficiency of my working device, it can be compared to the results from [10] in Appendix B. As seen in Figure B-1, the power conversion efficiency can be easily calculated from Figure 7 of [10]. The maximum power conversion efficiency from that reference work is 0.15%, as shown in Figure B-7.

We can also perform an EQE (external quantum efficiency) comparison calculation. The EQE of the device produced in [10] is quoted as being 17% +/- 3% for λ = 546nm at -1.5V for their hemispherical surface. But, a revised EQE calculation at 0V using their Figure 7 produces an EQE of 0.564%. This is similar to the EQE of my device being 0.538% at 0V.

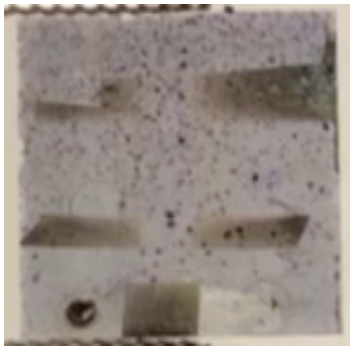

Figure 6-1: One of the two working devices. Of the four pixels visible here (not counting the base contact at the bottom), one of them functioned at 0.08% efficiency and the other three did not work (were shorted). Observe that the aluminum deposition pattern is the areas not covered by the shadow mask pattern depicted in Figure 3-4

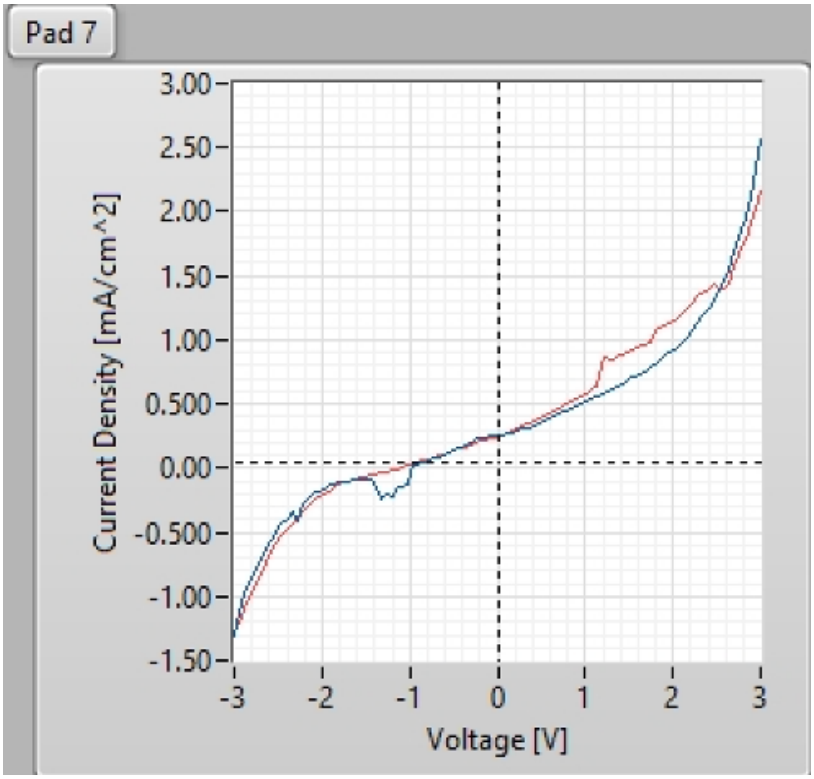

Figure 6-2: The overall J - V curve of one of the two working devices produced using the shadow mask method.

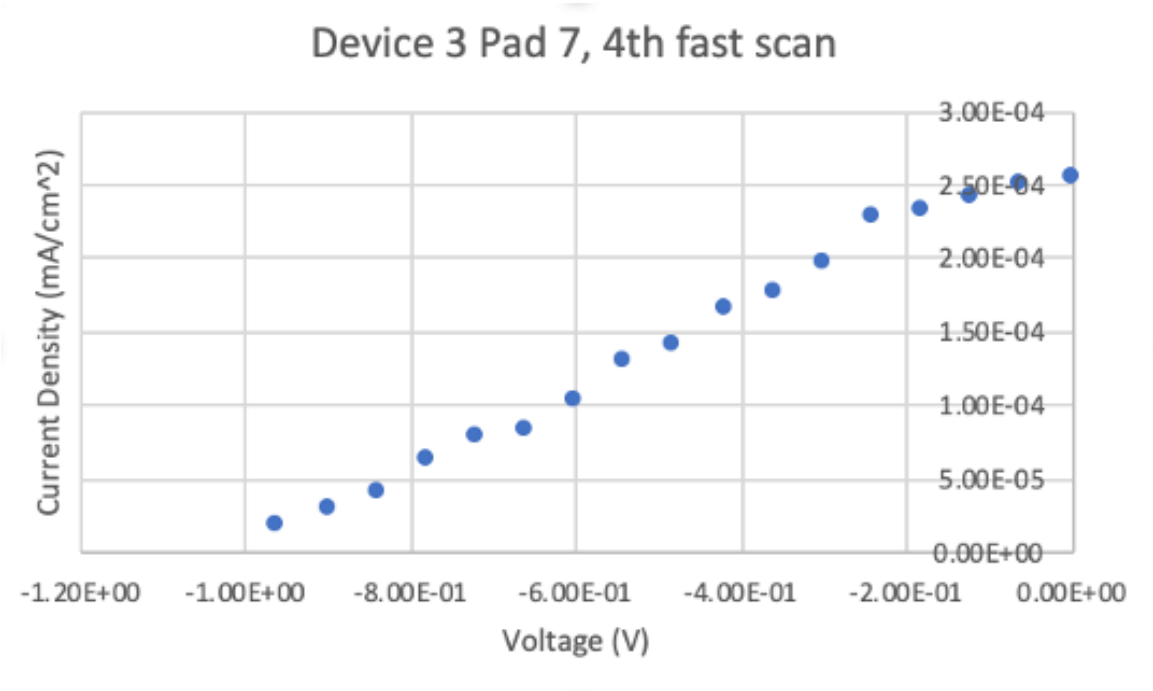

Figure 6-3: Details of the active (power producing) region of one of the two working devices produced using the shadow mask method. Using the calculation method for power shown in Appendix B, the power conversion efficiency of this device was shown to be 0.08%.

Overall, then, my device has superior performance, since I am illuminating my device using an AM1.5 spectrum (illumination designed to simulate the solar irradiance of a sunny day at 48.19 degrees north latitude, see [1]), while the device from [10] is only illuminating its device at a specific wavelength (546nm) and at a limited intensity (1.63 mW / cm^2, compared to the 100 mW / cm^2 of the AM1.5 standard). Thus, I have produced the first working AM1.5 solar cell with fully 3D printed information control.

Chapter 7

Future Work

One of the consistent limitations of fully 3D printed prior work has been the low quality electrical contacts, whose conductivity is inherently limited by their printed deposition process. By creating an alternative method of producing complex printed shapes with high metal quality, this thesis opens the door to several interesting applications, including incorporating printed light sensor arrays onto entirely 3D printed substrates, creating a 3D printed LED (an application which would very strongly benefit from a higher quality top metal contact), and possibly creating a "3D printed spherical camera" out of a network of 3D printed sensors.

Future work would be expected to improve the efficiency of this device to converge to the range more normally expected of non-printed PCDTBT-PCBM architectures (>5%), and to leverage those efficiency gains to produce high quality sensors which could capture useful information in a wide range of novel settings. Looking very far into the future, this method would be expected to compatible with a scaled up industrial process, since examples of large scale aluminum evaporated deposition for consumer products already exist.

Appendix A

ITO Slide Specifications

QUOTATION NO: 0304-14932
Page 1

THIN FILM DEVICES
1180 N. Tustin Ave.
Anaheim, CA 92807
TEL (714) 630-7127
FAX (714) 630-7119

DATE: March 4, 2019
SALES/TECHNICAL: Saleem Shaikh
SALES/MARKETING: Saleem Shaikh
SALES INSIDE: Katie Acosta
DELIVERY: 3-4 Weeks ARO

Visit our website at www.tfdinc.com

CUSTOMER:
MIT - Massachusetts Institute of Technology
Department of Mechanical Engineering
Cambridge, MA 02139

CONTACT: James Minor
TELEPHONE:
FAX:

EMAIL: JCMinor@mit.edu

PAYMENT ADDRESS:
THIN FILM DEVICES
P.O. Box 1841
Tustin, CA 92781-1841

TERMS: **1.)MasterCard/Visa only**
2.)Wire Transfer
3.)1% 10 days Net 30
w/Bank & Trade References
O.A.C.

P/N:554

ITEM	QTY	DESCRIPTION		UNIT PRICE	AMOUNT
		APPLICATION:	OPV/ R&D		
		Manufacture and coat per	Dwg Dated: 06/23/11 and the following:		
1.		**Substrate:**	TFD Supplied		
	200	Material:	Eagle XG	$4.95	$990
		Dimensions:	**0.495" x 0.495" ± 0.000" / 0.005"**		
		Thickness:	0.7mm		
		Surface:	60/40		
		Edges:	**Scribe & Break chips to MAXIMUM dimensions of 0.495"x 0.495"**		
2.		**COATING:**	Side 1		
		Material:	ITO		
		Thickness:	1450 ± 100Å		
		Resistivity:	20 ± 2 ohms/sq.		
		Transmission:	≥88% @ 550nm		
		Coating Defects:	60/40		
		Method:	Sputtering		
		Non-Uniformity:	± 2.5% across 14" x 18"		
		Tooling Mark Dimension:	None		
		NOTE:	**1. Surface Roughness of ITO ≤ 7Å RMS @ 1450Å** **2. Work function = -4.8eV -> -5.0eV**		
3.		**PATTERNING:**	Per Drawing P/N **554**		
4.		**NRE:**	Mylar Mask MIT **# 554**	N/C	
5.		**PACKAGING:**	STYROFOAM BOXES		
		QUALITY:	AS-9100 / ISO-9100 / MIL-I-45208		
		INSPECTION:	T%, Reflection: Mil-C-14806A, Adhesion, Abrasion: Mil-C-675 Mil-C-48497 Cosmetic: Mil-PRF-13830		
		NOTES:	**1.TFD prefers customer to supply their Carrier name and account number to Facilitate quicker delivery and to Avoid VAT charge.**		

Figure A-1: ITO order, page 1/3

			TFD PREFERS FEDEX ACCOUNT. 2. All coating specs disclosed in this quote, discussed prior on phone, or via Email is TFD confidential and proprietary. 3. PLEASE REFERENCE THIS QUOTE # ON YOUR PURCHASE ORDER. THANK YOU.		

TFD TERMS & CONDITIONS:

1.) FOR ALL TFD, INC., CUSTOMER'S "CONFIDENTIAL & PROPRIETARY" WRITTEN CONSENT IS NECESSARY BEFORE **ANY RELEASE OF TFD INFORMATION TO A 3RD PARTY, OTHER VENDORS,** (POTENTIAL COMPETION), **OR ANY FILM ANALYSIS ON TFD SUPPLIED PARTS OR PRODUCTS.**

2.) All Cancellations must be received within 7 working days after submitting PO and must be approved by TFD. Cancelled orders will be subject to charges according to material already purchased and level of completion.

3.) All return materials **must** get an RMA number from TFD prior to returning to TFD either for credit or replacement. All returns must have (NCR) reports.

4.) No Returns, RMA or credits will be allowed after receipt of the product later than 30 days except by written permission by TFD management.

5.) Consistent with standard industrial policies, TFD, Inc., assumes no liability for customer furnished material in the event of loss or damage.

6.) TFD will not be responsible for any failure of further processing of the part at customer or other vendor. Additional guarantee can be attained with acknowledgment of the future process at the buyer and third party location.

7.) TFD has a minimum order charge of $1050.00 on all orders. Exception to the Universities, and some TFD authorized sales for quoted prices.

8.) Terms for NRE charges are billed and due upon receipt or can be prepaid at time of placing purchase order.

9.) TFD requires a 5% overage of customer furnished material for testing and set-up purposes.

10.) Prices are premised on the right to ship over or under by 5%.

11.) Customer furnished material shall have beveled edges to minimize possibility of cracking or breaking.

12.) New customers please provide credit references with placement of purchase order. (3 trade, 1 bank)

13.) Foreign customers please provide a wire transfer of funds, letter of credit, or credit references for U.S.-based affiliate with placement of purchase order.

14.) Foreign customers, please provide Customs Broker name and address, Identification Number for customs purposes, and the FedEx Account Number for shipment, duties, and tax charges.

TERMS:

1). 1% 10 Days Net 30 on approved credit and 1 ½% interest will be charged on accounts past due.
2). Customers are required to provide a Fed Ex or UPS account number for orders shipped. Using your shipper account will lower your shipping charges, and may even qualify your company at a discounted rate.
3). Shipping charges will be added to the above price if shipped on TFD's account.

Figure A-2: ITO order, page 2/3

11/01/15

THIN FILM DEVICES, INC.

Dear Customer:

For past 30 years, TFD Inc. has evolved to be a foundery for different types of displays & medical devices such as MEM's, LCD, Oled, transparent heaters, EMI shield for medical products from prototype to mass production. In order to manufacture these devices, TFD has mature processes for **coatings** (IBS / CVD), **patterning** to 3.5 µm (370mm x 470mm area), **glass cutting**, dicing, **silk screening** and **packaging**. **Following are available:**

* **TCO's** such as ITO (5 types), IZO, AZO, FTO and (ITO:Al doped) with surface **smoothness** ≤ 7Å (rms) and **wf** ≥ 4.8 ev for ITO **(As IS Coated)** custom resistance/thicknesses available.
* PATTERNING: TFD can pattern with precision to as low as 3.5 µm line/space for as large as 370mm x 470mm area. We can pattern to 5 mask level for the product with highly precision alignment ±1 µm. TFD performs both Photo Etch & Lift Off processes.
  Bank formation (up to – 50 microns) using **SU-8, AZ 1500** and others also are available.
* WIRE MESH (IMBEDDED): There are several different wire mesh available in the market i.e. printed, and sputtered patterned. The TFD wire mesh is far superior and is imbedded into the PET or PEN film to 6 µm depth, so it is impervious to Acidic and basic harsh environments. Also, mechanically far superior. These films are commonly used for **Dye cell, aerospace heaters** and **P-caps.**
* INDEX MATCHED ITO (IMITO™): TFD pioneered and invented index matching concept to several key medium, liquid crystal, epoxy, air, etc. in 1987 IMITO™ is easily etchable, so it's highly applicable for **Pcap touch screens**, **EMI** shields, **LC** display panels, **LCOS**, and **LCD** heaters, while providing 0.5% average reflection (or less).
* OPTICAL COATINGS: BBAR and Hot Mirrors. Highly stable & durable and will meet/exceed salt & fog test, and 350° air temperature for ≥ 2 hours.
* ITO COLD PROCESS (LTITO): An ITO cold process **(≤60°C)** is applied for Plastic and Low Temperature polymer substrates such as color and EMI filters. Resistivity as low as 5 ohms/sq. at ≥85% transmission is achieved on PC, acrylic and polymers.
* BLACK MATRIX (Black Cr, Black Nb) or Black resin: coatings are a single-layer, sputtered film, rather than a multi-layer metal-oxide system; so the reflections through the glass are only 1% or less @ 550nm easily etch able. This coating is commonly used for optical window for displays and medical devices.
* LAMINATION: An excellent solution to ruggedization, which combines several key items for flat panel displays, EMI, sun filters, and heaters to be used for military or UL & OEM products.
* PRODUCTION CAPACITIES: TFD, Inc. has invested ≥ $ 30 Million over last 20 years (see website for production & QC equipment)
* GLASS FABRICATION: Cutting, beveling, dicing and shaping with full capability to provide any shape, for sizes to 24" x 24".
* QUALITY: AS 9100

Inquiry or requirements – email sales@tfdinc.com or call 714-630-7127

Sincerely,

Saleem Shaikh
President/Technical Sales

Figure A-3: ITO order, page 3/3

Appendix B

Prior Work Efficiency Calculation

Although [10] does not explicitly list its power conversion efficiency, that can be calculated from the data given in its figure 7, which will be shown several times in this appendix, along with the method for calculating power conversion efficiency.

Table B.1: Table 1

Entry	SecondEntry
ThirdEntry	FourthEntry

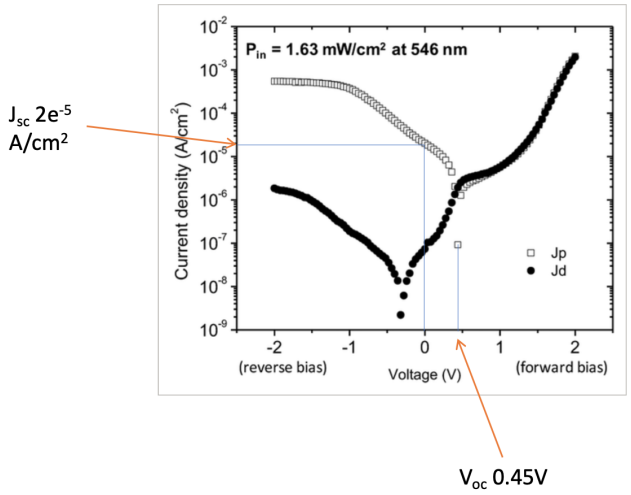

- P_{out} = Power Out
- J_{sc} = Short Circuit Current
- V_{oc} = Open Circuit Voltage
- FF = Fill Factor
- $P_{out} = J_{sc} * V_{oc} * FF$
- $P_{out} <= J_{sc} * V_{oc}$
- $P_{out} <= 9e^{-6}$ W/cm^2
- $P_{out} <= 9e^{-3}$ mW/cm^2
- P_{in} = 1.63 mW/cm^2
- Efficiency <= P_{out} / P_{in}
- Efficiency <= 0.55%

Figure B-1: Efficiency calculation method and upper bound.

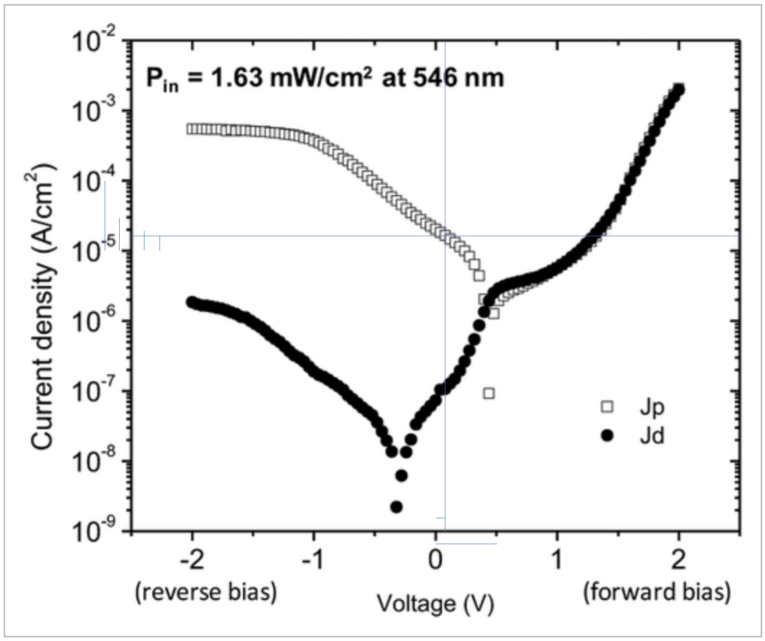

Factor Estimation

- By line lengths, V = 0.5V * 0.11 / 0.7 = 0.08V
- J is a log scale, so for reference it's 0.8" from 1e-5 to 1e-4 and 0.23" from 1e-5 to 2e-5, and (0.8/0.23) ~= ln10 / ln2
- So J = (e $^{[0.17*ln2/0.23]}$) *10^{-5} A/cm^2
- J = 1.7e^{-5} A/cm^2
- Efficiency = 0.08%

Figure B-2: Efficiency calculation, point 1.

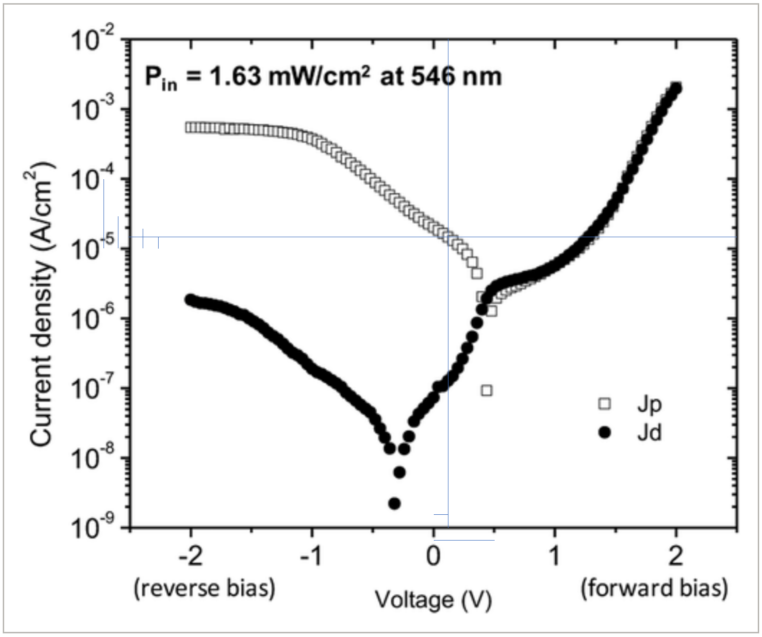

Factor Estimation

- By line lengths, V = 0.5V * 0.17 / 0.7 = 0.12V
- J is a log scale, so for reference it's 0.8" from 1e-5 to 1e-4 and 0.23" from 1e-5 to 2e-5, and (0.8/0.23) ~= ln10 / ln2
- So J = ($e^{[0.13*\ln 2/0.23]}$) $*10^{-5}$ A/cm²
- J = $1.5e^{-5}$ A/cm²
- Efficiency = 0.11%

Figure B-3: Efficiency calculation, point 2.

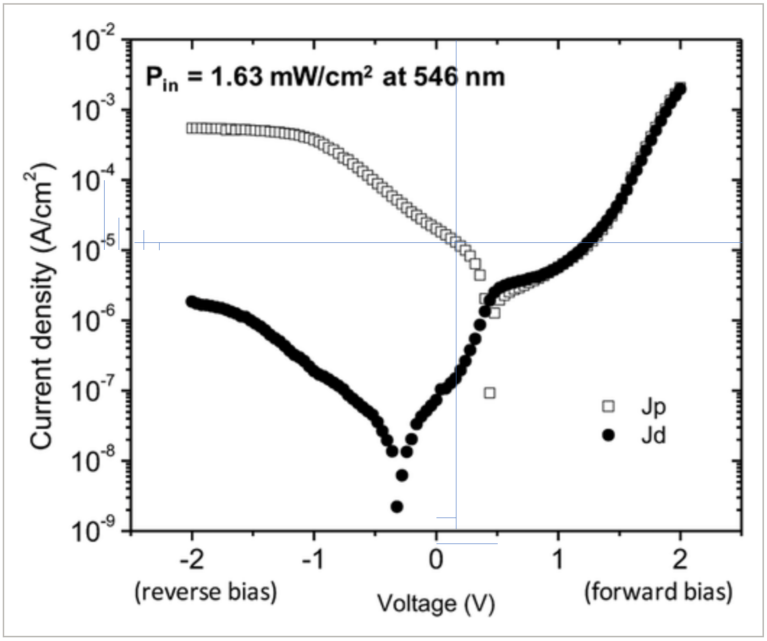

Factor Estimation

- By line lengths, V = 0.5V * 0.23 / 0.7 = 0.16V
- J is a log scale, so for reference it's 0.8" from 1e-5 to 1e-4 and 0.23" from 1e-5 to 2e-5, and (0.8/0.23) ~= ln10 / ln2
- So J = ($e^{[0.09*\ln 2/0.23]}$) $*10^{-5}$ A/cm²
- J = $1.3e^{-5}$ A/cm²
- Efficiency = 0.13%

Figure B-4: Efficiency calculation, point 3.

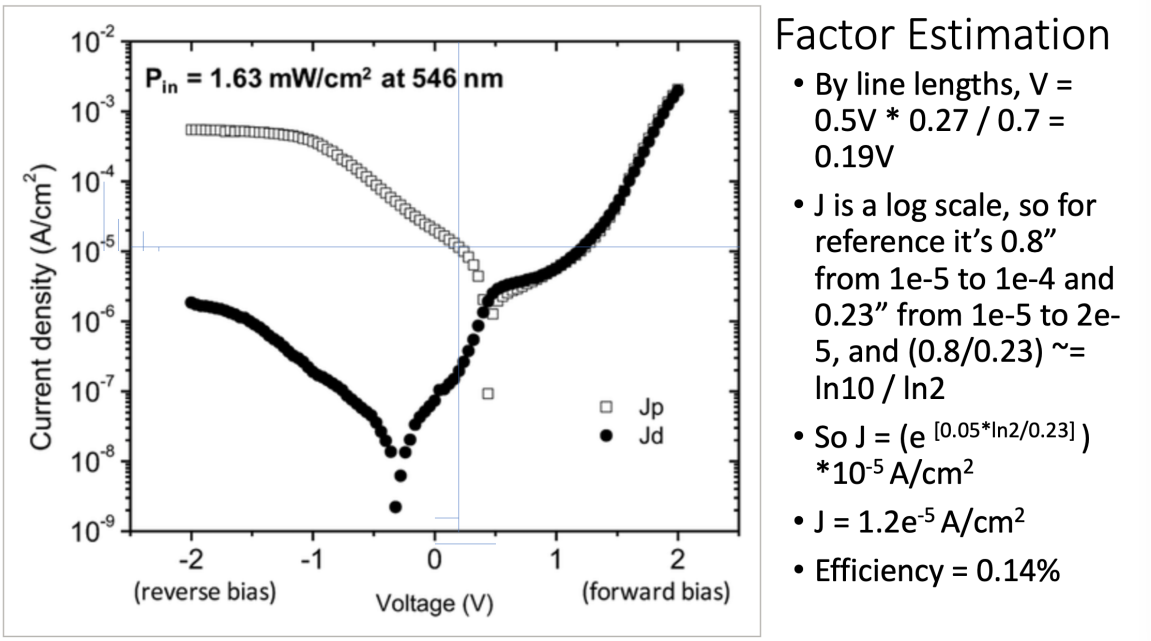

Figure B-5: Efficiency calculation, point 4.

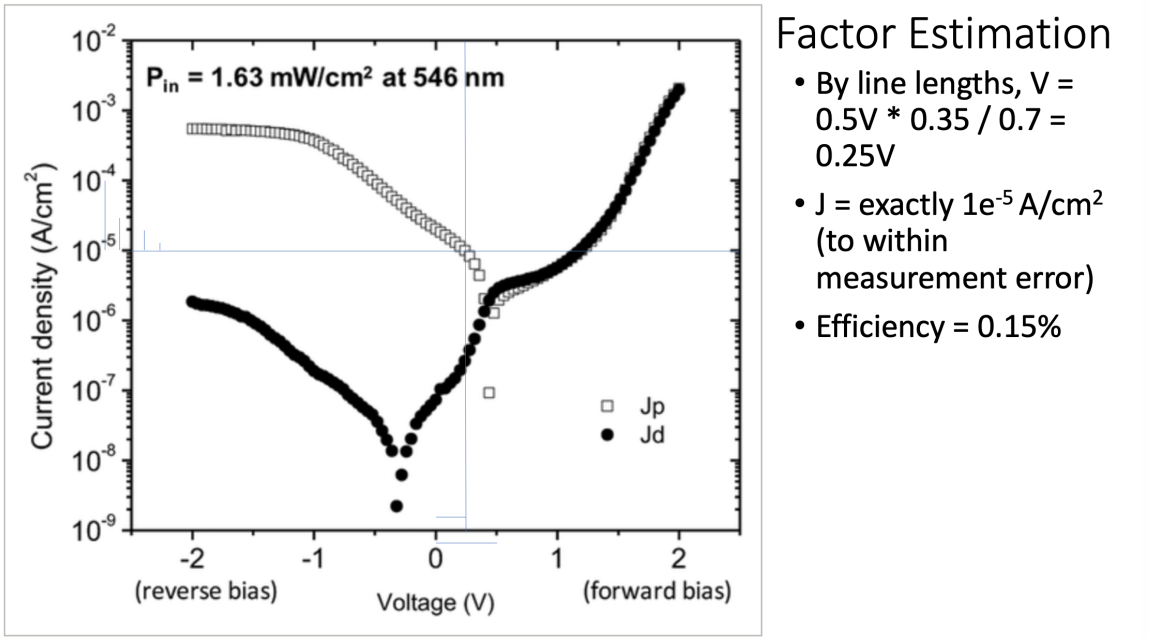

Figure B-6: Efficiency calculation, point 5.

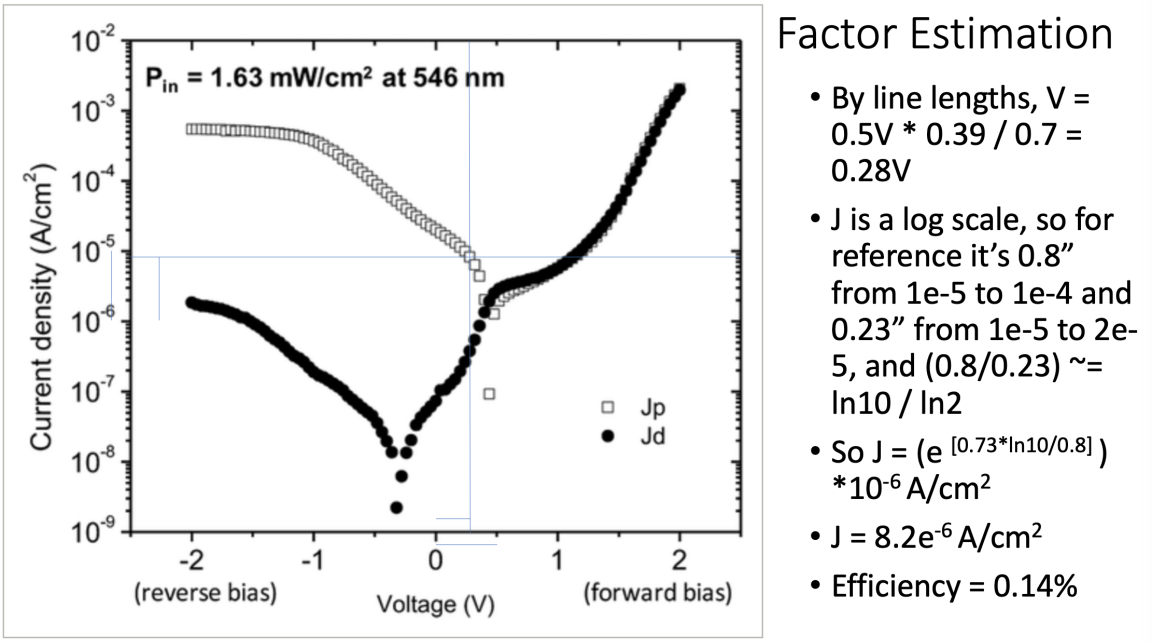

Figure B-7: Efficiency calculation, point 6. This is the maximum efficiency represented by the device.

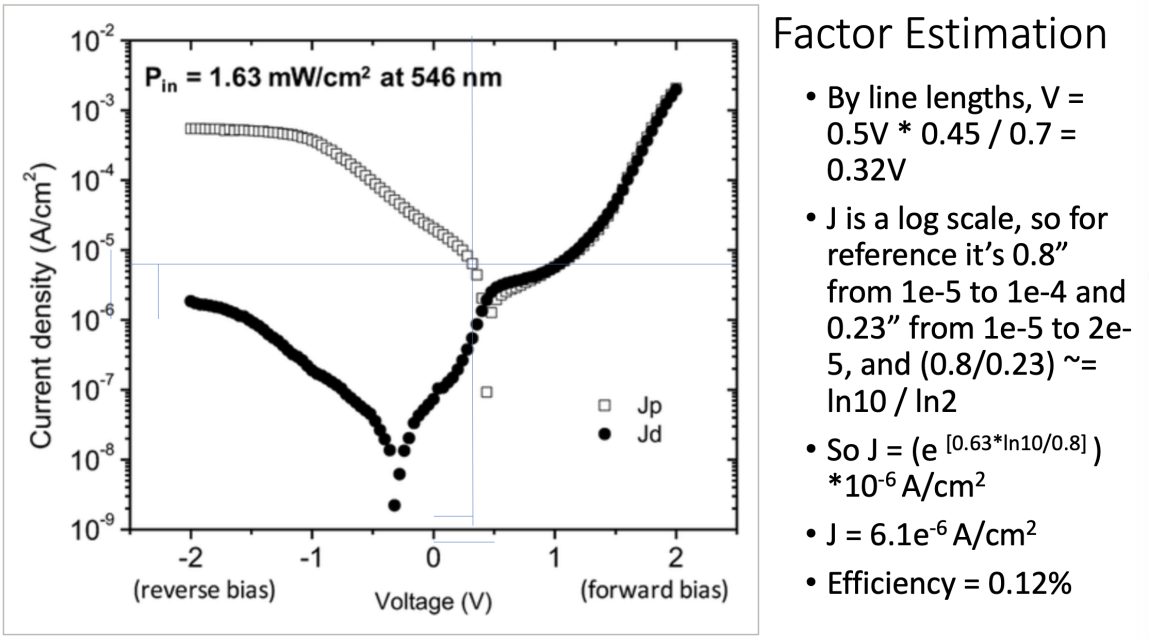

Figure B-8: Efficiency calculation, point 7.

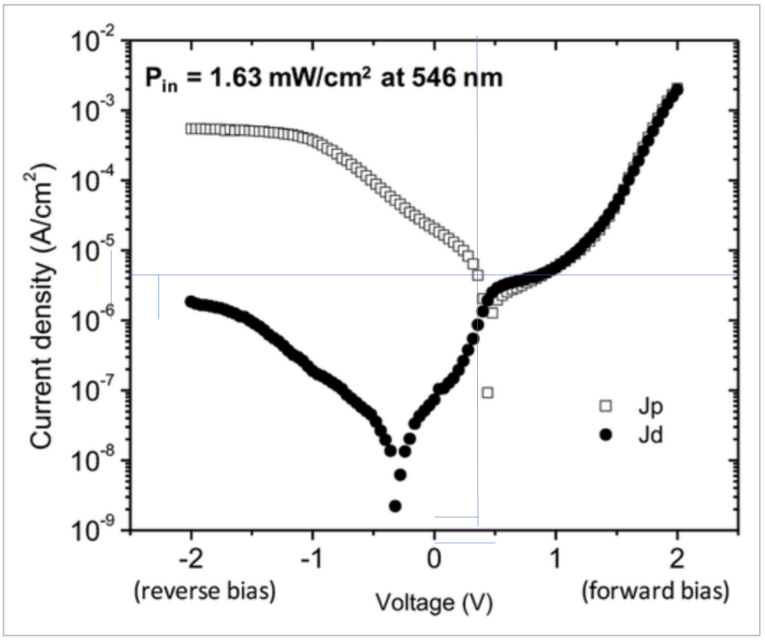

Factor Estimation

- By line lengths, V = 0.5V * 0.5 / 0.7 = 0.36V
- J is a log scale, so for reference it's 0.8" from 1e-5 to 1e-4 and 0.23" from 1e-5 to 2e-5, and (0.8/0.23) ~= ln10 / ln2
- So J = ($e^{[0.51*\ln 10/0.8]}$) *10^{-6} A/cm²
- J = 4.3e^{-6} A/cm²
- Efficiency = 0.09%

Figure B-9: Efficiency calculation, point 8.

Bibliography

[1] Reference solar spectral irradiance: Air mass 1.5. *https://rredc.nrel.gov/solar//spectra/am1.5/*.

[2] Dechan Angmo. Roll-to-roll inkjet printing and photonic sintering of electrodes for ito free polymer solar cell modules and facile product integration. *Advanced Energy Materials*, 3(2):172–175, 2013.

[3] G. Azzellino. Fully inkjet-printed organic photodetectors with high quantum yield. *Advanced Materials*, 25(47):6829–6833, 2013.

[4] Andreas Kornowski Claudia Pacholski and Horst Weller. Self-assembly of ZnO: from nanodots to nanorods. *Angewandte Chemie International Edition*, 41(7):1188–1191, 2002.

[5] Lionel Hirsch Dang, Minh Trung and Guillaume Wantz. P3HT: PCBM, best seller in polymer photovoltaic research. *Advanced Materials*, 23(31):3597–3602, 2011.

[6] Ralph Eckstein. Fully digitally printed image sensor based on organic photodiodes. *Advanced Optical Materials*, 6(5):1701108, 2018.

[7] Aniello Falco. Fully-sprayed and flexible organic photodiodes with transparent carbon nanotube electrodes. *ACS applied materials & interfaces*, 6(13):10593–10601, 2014.

[8] Stefan Gärtner. Eco-friendly fabrication of 4% efficient organic solar cells from surfactant-free P3HT: ICBA nanoparticle dispersions. *Advanced Materials*, 26(38):6653–6657, 2014.

[9] Sungjune Jung and Henry Sirringhaus. All-inkjet-printed, all-air-processed solar cells. *Advanced Energy Materials*, 4(14), 2014.

[10] Hyunsoo Kim. 3D printed masks and transfer stamping process to enable the fabrication of the hemispherical organic photodiodes. *Advanced Materials Technologies*, 2(9):1700090, 2017.

[11] Sanjeev J. Koppal. Toward wide-angle microvision sensors. *IEEE transactions on pattern analysis and machine intelligence*, 35(12):2982–2996, 2013.

[12] Illan J. Kramer and James C. Minor. Efficient spray-coated colloidal quantum dot solar cells. *Advanced Materials*, 2014.

[13] Illan J. Kramer and Gabriel Moreno-Bautista. Colloidal quantum dot solar cells on curved and flexible substrates. *Applied Physics Letters*, 105(16):163902, 2014.

[14] Gurunandan Krishnan and Shree K. Nayar. Towards a true spherical camera. *IS&T/SPIE Electronic Imaging*, 2009. International Society for Optics and Photonics.

[15] Paul Marks. 3d printing takes off with the world's first printed plane. *Science Direct*, 17(18), 2011.

[16] Xudong Guo Niu, Guangda and Liduo Wang. Review of recent progress in chemical stability of perovskite solar cells. *Journal of Materials Chemistry*, 3(17):8970–8980, 2015.

[17] Pattantyus-Abraham and Andras G. Depleted-heterojunction colloidal quantum dot solar cells. *ACS nano*, 4(6):3374–3380, 2010.

[18] Fabian Rengier. 3d printing based on imaging data: review of medical applications. *International journal of computer assisted radiology and surgery*, 5(4):335–341, 2010.

[19] Morten Schmidt. Spray coated indium-tin-oxide-free organic photodiodes with PEDOT: PSS anodes. *AIP Advances*, 4(10):107132, 2014.

[20] Helmut Neugebauer Serap Günes and Niyazi Serdar Sariciftci. Conjugated polymer-based organic solar cells. *Chemical reviews* , 107(4):1324–1338, 2007.

[21] Pitchaya Sitthi-Amorn and Wojciech Matusik. Multifab: a machine vision assisted platform for multi-material 3d printing. *ACM Transactions on Graphics (TOG)*, 34(4):129, 2015.

[22] Subramanian Sundaram. 3d-printed autonomous sensory composites. *Advanced Materials Technologies*, 2017.

[23] Mark D. Symes. Integrated 3d-printed reactionware for chemical synthesis and analysis. *Nature Chemistry*, 4(5):349–354, 2012.

[24] Jiechao Jiang Tao, Coby S. and Meng Tao. Natural resource limitations to terawatt-scale solar cells. *Solar Energy Materials and Solar Cells*, 95(12):3176–3180, 2011.

[25] Kaufui V. Wong and Aldo Hernandez. A review of additive manufacturing. *ISRN Mechanical Engineering*, 2012.